THE JOURNAL OF PHYSICAL CHEMISTRY B

ARTICLE

pubs.acs.org/JPCB

Two-Dimensional ^{1}H HYSCORE Spectroscopy of Dimanganese Di-μ-oxo Mimics of the Oxygen-Evolving Complex of Photosystem II

Sergey Milikisiyants, Ruchira Chatterjee, and K. V. Lakshmi*

Department of Chemistry and Chemical Biology and The Baruch '60 Center for Biochemical Solar Energy Research, Rensselaer Polytechnic Institute, Troy, New York 12180, United States

Supporting Information

ABSTRACT: The solar water-splitting protein complex, photosystem II, catalyzes one of the most energetically demanding reactions in nature by using light energy to drive water oxidation. The four-electron water oxidation reaction occurs at the tetranuclear manganese−calcium−oxo cluster that is present in the oxygen-evolving complex of photosystem II. The tetranuclear manganese−calcium−oxo cluster is comprised of mixed-valence Mn(III) and Mn(IV) ions in the ground state. The oxo−manganese dimer, $[H_2O(terpy)Mn^{III}(\mu\text{-}O)_2Mn^{IV}(terpy)OH_2](NO_3)_3$ (terpy = 2,2′:6′,2″-terpyridine) (**1**), is an excellent biomimetic model that has been extensively used to gain insight on the molecular structure and mechanism of water oxidation in photosystem II. In this work, weak magnetic interactions between the protons of the two terminal water ligands and the paramagnetic dimanganese "di-μ-oxo" core of **1** are quantitatively characterized using two-dimensional hyperfine sublevel correlation (HYSCORE) spectroscopy. For the water molecule that is directly coordinated at the Mn(III) ion, the two protons are found to be magnetically equivalent and exhibit near axial hyperfine anisotropy. In contrast, for the first time, we demonstrate that the two protons of the water molecule that is directly coordinated at the Mn(IV) ion are inequivalent. We obtain the isotropic and anisotropic components of the hyperfine interaction for each proton. A comparison of the HYSCORE spectra measured in the presence and absence of acetate ions provides unambiguous evidence that only one molecule of acetate binds to **1** by replacing a terminal water molecule that is coordinated at the Mn(III) ion.

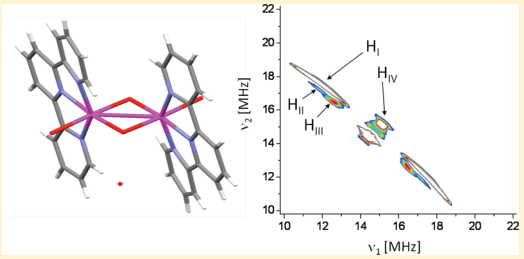

INTRODUCTION

The light-driven water oxidation reaction by the photosynthetic reaction center, photosystem II (PSII), is one of the most important chemical reactions in nature as it is the source of nearly all of the dioxygen that is present in the earth's atmosphere. The light-driven water oxidation reaction is catalyzed by the tetranuclear manganese−calcium−oxo (Mn_4Ca−oxo) cluster in the oxygen-evolving complex (OEC) of PSII. One of the major challenges in understanding the mechanism of the solar water oxidation reaction is elucidating the molecular structure of the Mn_4Ca−oxo cluster and the OEC of PSII. While X-ray crystallography studies provide a high-resolution structure of the PSII reaction center,[1−5] recent attempts to resolve the structure of the OEC have yielded insufficient resolution. In part, this is due to the difficulty in obtaining high-quality single crystals of PSII and also due to the observation that the higher valence manganese ions of the Mn_4Ca−oxo cluster of the OEC are reduced by the high-energy radiation that is used for X-ray crystallography.[6,7] Further, the high-resolution X-ray crystallography studies of the PSII reaction center only provide structural details on the dark ground state, known as the S_1 state of the OEC.[8] Although advanced spectroscopic techniques such as extended X-ray absorption fine structure (EXAFS) and electron paramagnetic resonance (EPR) spectroscopy have provided valuable insights on the Mn_4Ca−oxo cluster in the S_1 and higher S states of the OEC,[6,9−18] important structural details, such as the location and the coordination environment of the substrate water molecules that undergo oxidation, remain unknown. The magnetic interactions between the exchangeable protons of the water molecules and the unpaired electron spins within Mn_4Ca−oxo cluster have previously been investigated by electron−nuclear double resonance (ENDOR) and electron spin−echo envelope modulation (ESEEM) spectroscopy.[19−25] ENDOR and ESEEM spectroscopy have yielded quantitative electron−nuclear hyperfine parameters; however, the location and origin of the magnetically coupled exchangeable protons of bound water and/or hydroxo ligands of the Mn_4Ca−oxo cluster could not be inferred in these studies. This is in part due to the lack of experimental insight on the influence of the coordination geometry and oxidation state of the coordinating metal ion(s) on the electron−nuclear hyperfine interactions with the magnetically interacting protons.

Synthetic mixed-valence dimanganese "di-μ-oxo" dimers represent structurally well-defined molecular complexes that have been used as biomimetic model systems for the study of the OEC of PSII.[26,27] The influence of the coordination geometry and

Received: June 15, 2011
Revised: August 30, 2011
Published: September 30, 2011

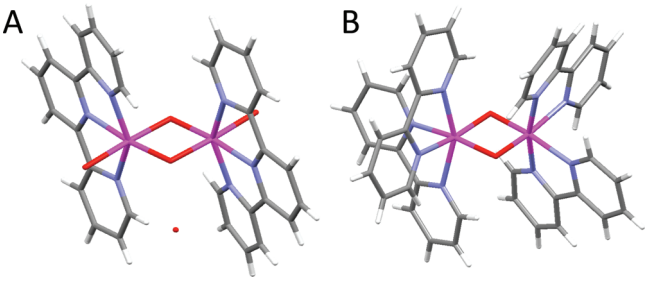

Figure 1. X-ray crystal structure of (A) $[H_2O(terpy)Mn^{III}(\mu\text{-}O)_2Mn^{IV}(terpy)OH_2](NO_3)_3$ (terpy = 2,2′:6′,2″-terpyridine) (**1**)[26] and (B) $[(bpy)_2Mn^{III}(\mu\text{-}O)_2Mn^{IV}(bpy)_2](ClO_4)_3$ (bpy = 2,2′-bipyridine) (**2**).[32] In the structure of complex **1**, the two manganese ions are bridged by di-μ-oxo bonds and each manganese ion is ligated to one molecule of terpyridine. Thus, there is an open coordination site on each manganese ion that is occupied by a directly coordinated water molecule. In the structure of complex **2**, the two manganese ions are once again bridged by di-μ-oxo bonds. However, each manganese ion is ligated to two bipyridine molecules that preclude the coordination of water molecules.

oxidation state of the coordinating manganese ion(s) on the electron−nuclear hyperfine parameters of dimanganese di-μ-oxo dimers can serve as a basis for interpretation of the EPR spectroscopic data of the OEC of PSII. Therefore, it is important to characterize the magnetic interactions of the unpaired electrons of the manganese ion(s) and surrounding protons of dimanganese di-μ-oxo model complexes.

The proton hyperfine interactions in mixed-valence dimanganese di-μ-oxo model compounds have previously been investigated by ENDOR and ESEEM spectroscopy.[28−31] The electron−nuclear hyperfine coupling parameters that were obtained in these studies detailed magnetic interactions with the protons and nitrogen atoms of the organic ligands of the dimanganese di-μ-oxo models. Despite immense biological relevance there is a lack of experimental data on the magnetic interactions of the protons of bound water ligands with the unpaired electron spins on the manganese ion(s) of dimanganese di-μ-oxo biomimetic models. To date, there is only one study that examines proton hyperfine parameters for water and methanol ligands of a dimanganese di-μ-oxo dimer using ENDOR and ESEEM spectroscopy.[29]

Among the synthetic dimanganese di-μ-oxo model compounds in literature, there are two complexes, $[H_2O(terpy)Mn^{III}(\mu\text{-}O)_2Mn^{IV}(terpy)OH_2](NO_3)_3$ (terpy = 2,2′:6′,2″-terpyridine) (**1**)[26,27] and $[(bpy)_2Mn^{III}(\mu\text{-}O)_2Mn^{IV}(bpy)_2](ClO_4)_3$ (bpy = 2,2′-bipyridine) (**2**)[32] (Figure 1), that are of particular interest as biomimetic models. **1** and its derivatives are excellent and extensively studied biomimetic models of the OEC of PSII. The presence of a terminal water ligand that is coordinated to each manganese ion in the dimanganese di-μ-oxo core of **1** makes this a compound of great structural relevance and provides an important basis for elucidating the molecular and electronic structure of the OEC of PSII. Moreover, upon chemical and possibly electrochemical oxidation, **1** acts as a functional water oxidation catalyst.[26,27,33] Understanding the mechanism of water oxidation by **1** is of fundamental interest as it could play a crucial role in elucidating the mechanistic details of water oxidation by the OEC of PSII. The importance of **2** arises from its structural similarity with **1**; the most pronounced difference between the complexes is the absence of an open coordination site on the manganese ion(s) in the dimanganese di-μ-oxo core of complex **2** for the binding of terminal water ligands. The structural similarity of **1** and **2** with the presence and absence of coordinating terminal water ligands, respectively, provides an excellent frame of reference to understand chemical and spectroscopic properties of the terminal water ligands of **1**.

In this study, we perform two-dimensional (2D) proton (^1H) hyperfine sublevel correlation (HYSCORE) spectroscopy to characterize magnetic interactions between the unpaired electrons of the manganese ion(s) in the dimanganese di-μ-oxo core and the surrounding proton nuclear spins of **1** and **2**.

In comparison with one-dimensional (1D) spectroscopic techniques such as ENDOR and ESEEM, 2D HYSCORE spectroscopy has superior resolution for multinuclear systems as the nuclear frequencies corresponding to different electron spin manifolds are dimensionally separated in 2D frequency space. Further, using a combination of deuterium exchange of the protons of the terminal water molecules, the measured proton hyperfine parameters, and comparison of the spectroscopic data for **1** and **2**, we unambiguously assign the observed protons to the coordinating water molecules and organic ligands of **1**, respectively.

This study provides, for the first time, characterization of the hyperfine interactions of the protons of the terminal water molecules that are coordinated at both Mn(IV) and Mn(III) ions. This is of critical importance for the interpretation of spectroscopic data obtained from mixed-valence multinuclear manganese systems, such as the OEC of PSII. Further, using 2D ^1H and ^{13}C HYSCORE spectroscopy, we identify the metal site where an acetate ion binds in complex **1**.

MATERIALS AND METHODS

Syntheses of Biomimetic $[OH_2(terpy)Mn^{III}(\mu\text{-}O)_2Mn^{IV}(terpy)OH_2](NO_3)_3$ and $[(bpy)_2Mn^{III}(\mu\text{-}O)_2Mn^{IV}(bpy)_2](ClO_4)_3$ Model Complexes. The chemicals for the syntheses of $[OH_2(terpy)Mn^{III}(\mu\text{-}O)_2Mn^{IV}(terpy)OH_2](NO_3)_3$ (**1**) (terpy, 2,2′:6′,2″-terpyridine) and $[(bpy)_2Mn^{III}(\mu\text{-}O)_2Mn^{IV}(bpy)_2](ClO_4)_3$ (**2**) (bpy, 2,2′-bipyridine) were purchased from Sigma and used without further purification. The synthesis followed the literature protocol previously published by Brudvig, Crabtree, and co-workers[26] for the synthesis of **1** and Cooper and Calvin[32] for the synthesis of **2**. Continuous-wave EPR and electron-spin−echo detected field-sweep EPR spectroscopy of both **1** and **2** yielded a characteristic multiline EPR signal for a mixed-valence Mn(III)Mn(IV) dimer with ∼16 lines centered at $g \sim 2$ (Figure 2). The EPR studies of **1** were conducted in both protonated and deuterated aqueous buffer containing 0.1 M potassium nitrate (KNO_3), 5 mM terpy at pH 4.3 and pH 3.8 for protonated[34] and deuterated buffer, respectively. The pH of the buffers was adjusted with dilute nitric acid (HNO_3) and potassium hydroxide (KOH). Methanol (10%) was added as a cryoprotectant for the low-temperature EPR spectroscopy measurements. The EPR spectroscopy studies of **1** were also conducted in buffer containing either natural abundance or ^{13}C-labeled 1 M sodium acetate ($CH_3{}^{13}COONa$) (Cambridge Isotope Laboratories, Andover, MA) at pH 4.5, referred to as "acetate buffer" in this study. The pH of the ^{13}C-labeled acetate buffer was adjusted with ^{13}C-labeled acetic acid ($CH_3{}^{13}COOH$) (Cambridge Isotope Laboratories, Andover, MA). The EPR spectroscopy studies of **2** were conducted in a 2:1 acetonitrile and dichloromethane solvent mixture.

EPR Spectroscopy. The X-band EPR spectra were recorded on a custom-built cw/pulsed X-band Bruker Elexsys 580 spectrometer (Bruker BioSpin, Billerica, MA). The pulsed EPR spectroscopy measurements were conducted with a dielectric flex-line probe ER 4118-MD5 (Bruker BioSpin, Billerica, MA), and a dynamic continuous-flow cryostat CF935 (Oxford Instruments, Oxfordshire, U.K.) was used for cryogenic measurements. The operating microwave frequency of the pulsed resonator was 9.71 GHz, and all of the spectra were acquired at 5 K. The 2D HYSCORE spectra of **1** and **2** were recorded at magnetic field positions of 3393 and 3382 G, respectively.

A 6-pulse HYSCORE sequence was used for the acquisition of the 2D ^{1}H HYSCORE spectra.[35,36] For the 6-pulse 2D HYSCORE sequence, the echo amplitude was measured with the pulse sequence $(\pi/2)_y-\tau_1-(\pi)_y-\tau_1-(\pi/2)_x-t_1-(\pi)_x-t_2-(\pi/2)_x-\tau_2-(\pi)_x-\tau_2-(\text{echo})_x$. The interpulse delays were defined as the difference between the starting points of the pulses. The echo intensity was obtained by integration over the 8 ns detector gate and measured as a function of t_1 and t_2, where t_1 and t_2 were incremented in steps of 24 ns from the initial values of 32 and 40 ns, respectively. Equal amplitude pulses of 8 ns for $\pi/2$ and 16 ns for π were used to record a 256 × 256 matrix. The 8 ns time difference between the initial value of the time delays, t_1 and t_2, and the $\pi/2$ and π pulses was used to account for the difference in length between the $\pi/2$ and π pulses to obtain symmetric spectra. Since the blind spot pattern in a 6-pulse 2D HYSCORE spectrum is determined by the τ_1 and τ_2 delays, the experimental measurements were performed with multiple delay values of τ_1 and τ_2; the values are provided in the figure legends. The application of an 8-step phase cycling procedure was used to eliminate the unwanted echoes.[35]

For both **1** and **2**, at the corresponding spectral positions there are multiple orientations that contribute to the 2D ^{1}H HYSCORE spectrum. This results in characteristic cross-peaks that appear as extended ridges in the 2D HYSCORE spectrum.[37] In addition, a 6-pulse HYSCORE spectrum has a blind spot pattern determined by interpulse delays, τ_1 and τ_2, respectively. The values of the interpulse delays, τ_1 and τ_2, modulate the intensity distribution over the entire 2D frequency space; thus, the choice of these interpulse delays is critical in resolving hyperfine interactions in the measured 2D ^{1}H HYSCORE spectra. While for weaker hyperfine interactions, it is advantageous to set the interpulse delays to blind spot the corresponding hyperfine interactions from "nonspecific" matrix nuclei, the result is that ridges arising from the stronger hyperfine interactions may appear segmented for different interpulse delays, τ_1 and τ_2, used in the pulse sequence.

We also investigated the application of a 4-pulse HYSCORE sequence in this study. The use of a 4-pulse HYSCORE sequence resulted in (i) strong suppression of the ^{1}H cross-peaks due to very strong signal modulations arising from the ^{14}N nuclei and (ii) the presence of unwanted internuclear combination peaks which overlap with the ^{1}H cross-peaks. The cross-suppression effect arises from the fact that the observed 2D HYSCORE signal is a multiplication product of both strongly modulating nuclei, such as ^{14}N, and weakly modulating nuclei, such as protons.[38] In this case, the strongly modulating nuclei cause partial or complete suppression of signals from weakly modulating nuclei that are coupled to the same electron spin.[38] Since hyperfine couplings to the protons are of particular interest in this study, we use a 6-pulse ^{1}H HYSCORE sequence[35] to alleviate the impact of cross-suppression from the presence of the ^{14}N nuclei. Both of the unwanted effects, namely, cross-suppression and internuclear cross-peaks, were absent in the 6-pulse HYSCORE spectroscopy experiments resulting in clearly interpretable proton spectra.

The 6-pulse HYSCORE spectra were processed using Matlab R2008a. The echo decay was eliminated by a low-order polynomial baseline correction and tapered with a Gaussian function. Prior to 2D Fourier transformation, the data was zero filled to a 2048 × 2048 matrix and the magnitude spectra were calculated. The 2D HYSCORE spectra are presented as contour plots using the "contour" function of Matlab R2008a software.

Analysis of the 2D ^{1}H and ^{13}C HYSCORE Spectra. The three principal components of an electron−nuclear hyperfine tensor can be presented as $(A_x, A_y, A_z) = (a_{iso} - T(1-\delta), a_{iso} - T(1+\delta), a_{iso} + 2T)$ where a_{iso}, T, and δ are the isotropic, dipolar, and rhombic components of the hyperfine tensor, respectively. In the case of axial symmetry ($\delta = 0$, $A_x = A_y = A_\perp = a_{iso} - T$, $A_z = A_\parallel = a_{iso} + 2T$), the ^{1}H or ^{13}C cross-peaks (which appear as ridges in powder samples) represent straight line segments when plotted in frequency-squared coordinates.[37] In this case, the anisotropic and isotropic components of the electron−nuclear hyperfine interaction can be obtained from the slope and the intercept of the ridges.[37] Based on the values of the slope, $Q_{\alpha(\beta)}$, and the intercept, $G_{\alpha(\beta)}$, that are determined experimentally and the calculated value of the nuclear Zeeman frequency, ν_I, the values of a_{iso} and T can be calculated from following equations:[39]

$$T = \pm\sqrt{\frac{16}{9(1-Q_{\alpha(\beta)})}\left\{G_{\alpha(\beta)} + \frac{4\nu_I^2 Q_{\alpha(\beta)}}{1-Q_{\alpha(\beta)}}\right\}} \quad \text{and}$$

$$a_{iso} = \pm 2\nu_I\frac{1+Q_{\alpha(\beta)}}{1-Q_{\alpha(\beta)}} - \frac{T}{2} \qquad (1)$$

To obtain the values $Q_{\alpha(\beta)}$ and $G_{\alpha(\beta)}$, the frequency-squared coordinates of the points were measured on the median of a ridge corresponding to the highest signal intensity along the direction of the ridges. This is appropriate since the processes responsible for line broadening in the 2D frequency space (e.g., nuclear relaxation, hyperfine strain, and signal apodization) would not affect the position of maximum signal intensity. Similarly, a small rhombicity, δ, of the hyperfine tensor in the first approximation does not alter the position of the median of the ridge, and thus it would not affect the quality of the analysis. The measured coordinates were fit with a straight line using a least-squares algorithm which yielded the values of $Q_{\alpha(\beta)}$ and $G_{\alpha(\beta)}$. Each pair of $Q_{\alpha(\beta)}$ and $G_{\alpha(\beta)}$ values results in four sets of possible hyperfine parameters (see eq 1), where the sign of T can be positive or negative, and for a given value of T, there are two possible values of a_{iso}. Numerical simulations of the experimental 2D HYSCORE spectra using the hyperfine parameters obtained from the linear analyses were performed using the "saffron" function of the EasySpin software package.

To estimate the errors of the hyperfine parameters obtained in this study, the admissible variations of values of the slope and the intercept $Q_{\alpha(\beta)}$ and $G_{\alpha(\beta)}$ were estimated by considering various points in the middle of the ridges, and the variation of the amplitude of the hyperfine parameters that were obtained were taken as the error bars.

RESULTS

Figure 2A−C shows the electron-spin−echo detected field-sweep EPR spectrum of **1** in aqueous buffer and acetate buffer

and **2** in an ACN/CH_2Cl_2 solvent mixture, respectively. All three EPR spectra display a "16-line pattern" that is characteristic of a mixed-valence Mn(III)Mn(IV) state of the dimanganese di-μ-oxo core of **1** and **2**.[40,41] The 16-line pattern of the EPR spectra is determined by the electron−nuclear hyperfine interaction between unpaired electrons on the manganese ions and the nuclear spin of ^{55}Mn ($I = 5/2$). In the spectra displayed in Figure 2A−C, the weak magnetic interactions with the surrounding proton nuclei of **1** and **2** are masked by inhomogeneous broadening of the EPR resonances and consequently remain unresolved in the EPR spectra.

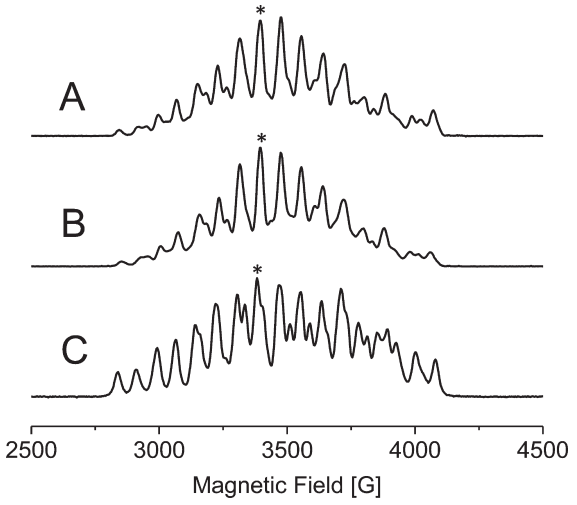

Figure 2. Electron-spin−echo detected field-sweep EPR spectrum of (A) **1** in protonated buffer (B) **1** in acetate buffer and (C) **2** in 2:1 CH_3CN:CH_2Cl_2, respectively. The asterisk marks the position of the magnetic field that was used for the 2D ^{1}H HYSCORE measurements.

In order to probe the weak magnetic interactions with the surrounding protons, we perform 2D ^{1}H HYSCORE spectroscopy measurements of **1** and **2**. The 2D ^{1}H HYSCORE spectra were acquired at magnetic field values corresponding to the highest intensity of the spin−echo spectrum that is marked with an asterisk in Figure 2A−C. Figure 3A shows the 2D ^{1}H HYSCORE spectrum of **1** in aqueous buffer. We observe multiple features that are located at the proton Zeeman frequency (14.45 MHz) that are symmetric with respect to the main diagonal of the 2D ^{1}H HYSCORE spectrum in Figure 3A. We assign these features to partially overlapped cross-peaks or ridges arising from electron−nuclear hyperfine interactions with four distinct groups of protons (H_I−H_{IV}) (indicated by arrows in Figure 3A).

The most pronounced pair of ridges in Figure 3A is assigned to hyperfine interaction with the H_I group of protons. There are two

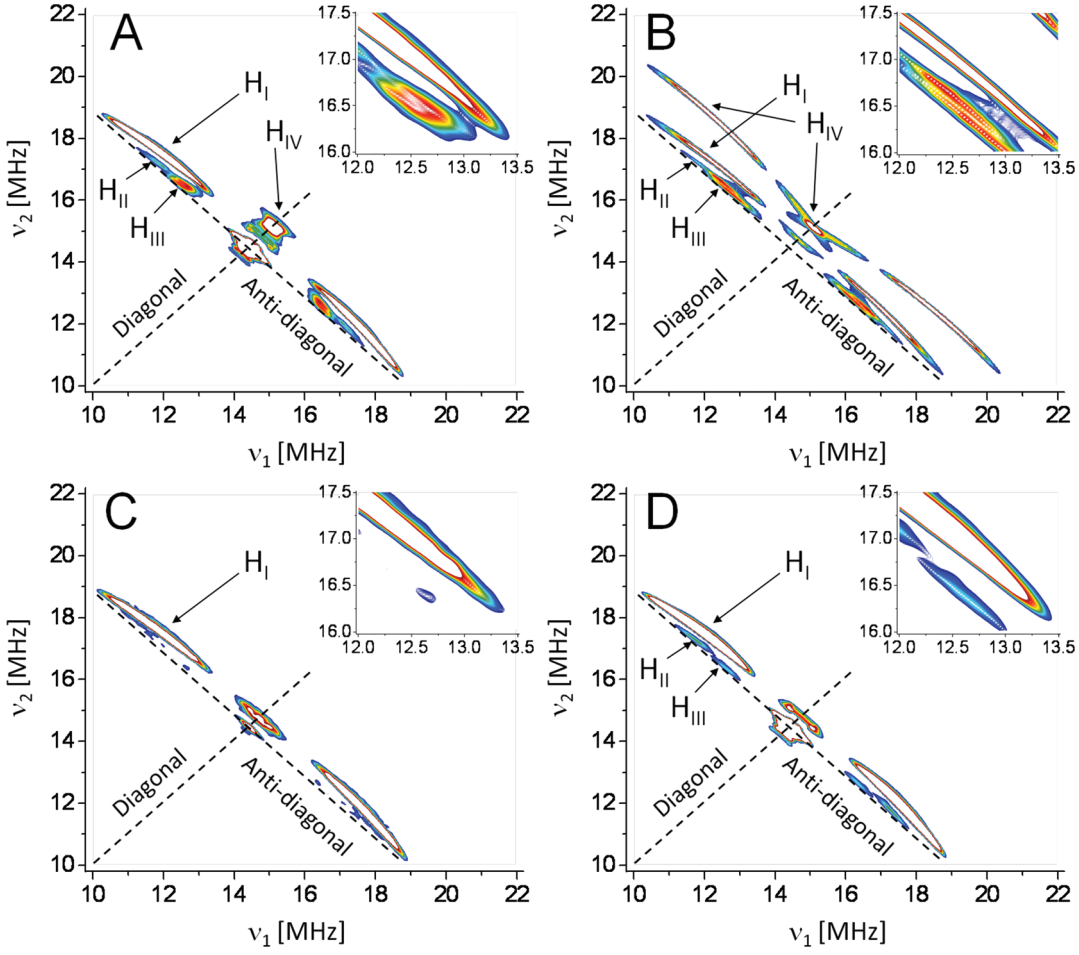

Figure 3. 2D ^{1}H HYSCORE (A) spectrum of **1** in protonated aqueous buffer at pH 4.3, (B) simulated spectrum of **1** in protonated aqueous buffer, (C) spectrum of **1** in deuterated aqueous buffer at pH 3.8, and (D) spectrum of **1** in acetate buffer at pH 4.5. All of the spectra were obtained with interpulse delays, τ_1 and τ_2, of 28 and 140 ns, respectively.

weaker pairs of ridges that are located very close to each other, and these can be distinguished by the slightly different shift from the antidiagonal (see inset of Figure 3A). The pairs with a larger and smaller shift from the antidiagonal are assigned to the H_{II} and H_{III} group of protons, respectively. In addition to the features that are separated with respect to the main diagonal, we observe two well-pronounced features that are located on the diagonal itself. The feature that is located at 14.45 MHz (at the crossing point of the diagonal and antidiagonal) is easily recognized as arising from hyperfine interactions with nonspecific matrix protons. The second feature on the diagonal that has the largest shift from the antidiagonal is due to hyperfine interactions with a distinct group of protons, H_{IV}. The significant shift from the antidiagonal indicates that the hyperfine interaction with the H_{IV} group of protons is largely anisotropic in nature.

To better resolve the ridges corresponding to the hyperfine interaction with the H_{IV} group of protons, we measure additional 2D ^{1}H HYSCORE spectra with varying interpulse delays, τ_1 and τ_2. Figure 1SA shows the 2D ^{1}H HYSCORE spectrum with τ_1 and τ_2 delays of 28 and 112 ns, respectively. For these interpulse delays, the spectrum is dominated by an unresolved diagonal feature due to presence of hyperfine interactions with the matrix protons. The overall width of the feature is ~4 MHz which represents the maximum size of the hyperfine interaction with the matrix protons. Most importantly, at these interpulse delays, the nondiagonal segments of the ridges due to hyperfine interactions with the H_{IV} group of protons are pronounced, and these can be detected unambiguously. The nondiagonal features of the ridges are also observed in a spectrum that is measured with τ_1 and τ_2 delays of 68 and 452 ns, respectively, which is shown in Figure 2S. In this case, the application of a lengthy τ_2 delay causes frequent repetition of the blind spot, which divides the ridges into several segments. However, there are two pairs of ridges corresponding to the hyperfine interaction with H_{IV} that can be detected in this spectrum. This provides valuable information on the precise location of the ridges in 2D frequency space.

Using linear analysis of the ridges arising from the hyperfine interactions, we determine the possible sets of hyperfine parameters for each of the four groups of protons, namely, H_I−H_{IV}. The parameters that are obtained from the linear analyses are listed in Table 1S. As can be seen in Table 1S, each pair of $Q_{\alpha(\beta)}$ and $G_{\alpha(\beta)}$ values results in four sets of possible hyperfine parameters (see Materials and Methods section). It is not feasible to discriminate between the four sets of possible hyperfine parameters solely on the basis of spectroscopic data. The origin of this uncertainty is due to the independence of the position of the ridges on interchange of the parallel and perpendicular components of the hyperfine interaction as well as simultaneous change of their signs. Thus, to discriminate between the sets of the hyperfine parameters, the parameters that are obtained in this study have to be considered in combination with the electronic and molecular structure of the dimanganese di-μ-oxo complexes (see Discussion section).

To confirm our assignments of the observed spectroscopic features, we perform numerical simulations of the experimental 2D ^{1}H HYSCORE spectrum in Figure 3A. The simulations are performed using the first set of the parameters listed in Table 1S. The simulated spectrum is shown in Figure 3B. We successfully reproduce the spectral features that are observed in the experimental 2D ^{1}H HYSCORE spectrum in Figure 3A. Some of the features of the simulated 2D ^{1}H HYSCORE spectrum (Figure 3B) are not present in the experimental spectrum (Figure 3A). Such discrepancies likely arise from nonideality of microwave pulses in the experimental spectrum contrary to the assumption of ideal pulses that is used for the simulations.

From the X-ray crystal structure of **1** (Figure 1A),[26] it is known that (a) the protons of the terpyridine ligand are located at distances ranging from 3.14 to 7.65 Å from the two manganese ions, (b) there are two terminal water molecules that are directly coordinated to the dimanganese di-μ-oxo core, and (c) there is one water molecule that is hydrogen-bonded (H-bonded) to the oxygen atom of a μ-oxo bridge. Thus, the hyperfine interactions that are observed with the protons H_I−H_{IV} arise either from the terpyridine ligand or from the directly coordinated/surrounding water molecules. To discriminate between these two possibilities, we measure the 2D ^{1}H HYSCORE spectra of **1** in deuterated buffer (Figure 3C). The experimental parameters that were used in the acquisition of this spectrum are identical to the parameters that were used for the spectrum of **1** in protonated buffer. As seen from the comparison of the 2D ^{1}H HYSCORE spectra in Figure 3A and C, the cross-peaks or ridges arising from hyperfine interactions with the H_{II}, H_{III}, and H_{IV} group of protons completely disappear upon deuterium exchange. However, the pair of ridges arising from hyperfine interaction with the H_I group of protons remains virtually unchanged with deuterium exchange. Thus, we conclude that H_{II}, H_{III}, and H_{IV} arise from hyperfine interactions with exchangeable protons on the water molecules while H_I is attributed to hyperfine interactions with nonexchangeable protons of the terpyridine ligand of **1**.

To further support this conclusion, we measure the 2D ^{1}H HYSCORE spectrum of **2** under identical experimental conditions. In **2**, the manganese ions are coordinated by four bipyridine ligands and two μ-oxo bridges.[32] However, **2** does not contain terminal water molecules that are directly coordinated to either of the manganese ions. The distances and angles between the closest protons on the bipyridine ligands and the manganese ions of **2** are very similar to those of **1** (Figure 1A−B). The 2D ^{1}H HYSCORE spectrum of **2** is shown in Figure 3S. Only one pronounced ridge, similar to that arising from the hyperfine interaction with the H_I group of protons of **1**, is observed in the spectrum. This observation is in agreement with our assignment of H_I to hyperfine interactions with the intrinsic protons of the terpyridine ligand and H_{II}−H_{IV} to interactions with the water protons in Figure 3A. From the slope and the intercept of the ridge of **2** in frequency-squared coordinates (not shown), we obtain isotropic and anisotropic hyperfine parameters, $a_{iso} = -0.13$ MHz, −4.4 MHz and $T = \pm 4.5$ MHz, respectively.

To obtain additional insight on the nature of the hyperfine interactions with the H_{II}−H_{IV} group of protons, we measured the 2D ^{1}H HYSCORE spectrum of **1** in acetate buffer. It has previously been suggested that acetate directly binds to one of the manganese ions by replacing the corresponding terminal water molecule that is coordinated to a manganese ion in the dimanganese di-μ-oxo core of **1**.[34,42] The 2D ^{1}H HYSCORE spectrum of **1** in acetate buffer is shown in Figure 3D. A comparison of the spectrum in Figure 3D with the spectrum shown in Figure 3A clearly indicates that ridges H_I−H_{III} remain virtually unchanged, while ridge H_{IV} completely disappears. We do not observe the appearance of additional proton ridges in the spectrum in Figure 3D. Thus, we conclude that the hyperfine interaction with the H_{IV} group of protons is from the water molecule that is replaced upon the binding of acetate to **1**.

Once again, to better resolve the ridges corresponding to the hyperfine interaction with the protons, we measure additional

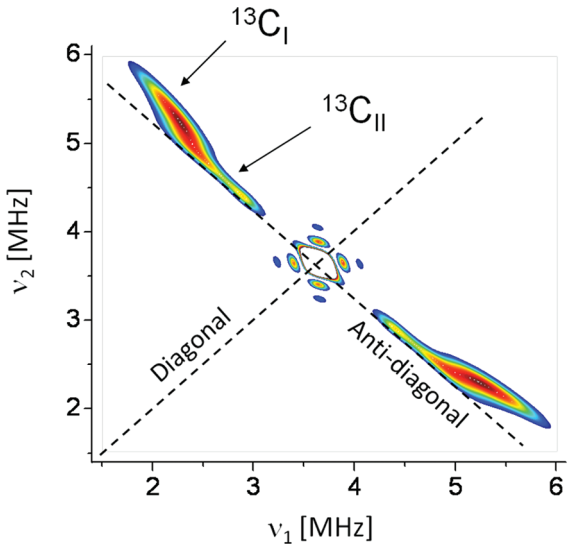

Figure 4. 2D ^{13}C difference HYSCORE spectrum of **1** in ^{13}C-labeled and natural abundance acetate buffer. The spectrum was obtained with interpulse delays, τ_1 and τ_2, of 68 and 100 ns, respectively.

spectra of **1** in acetate buffer with varying interpulse delays. Figure 1SB shows the 2D ^1H HYSCORE spectrum of **1** in acetate buffer with τ_1 and τ_2 delays of 28 and 112 ns, respectively. Comparison of the spectrum in Figure 1SB with a spectrum of **1** that was measured under identical experimental conditions in aqueous protonated buffer (Figure 1SA) provides clear evidence that H_{IV} disappears if acetate is added to the solution. Table 2S lists the possible sets of hyperfine parameters that are obtained from the linear analysis of the ridges arising from the hyperfine interactions with the H_I−H_{III} groups of protons in Figure 3D.

Figure 4S shows the 2D difference ^1H HYSCORE spectrum of **1** in protonated and acetate buffer. There are three spectral features that are present in this spectrum. The most pronounced spectral feature that is located on the diagonal is also clearly observed in the protonated spectrum (Figure 3A). The weaker spectral feature, located very close to the antidiagonal, belongs to the same pair of ridges, but it was not observed in the protonated spectrum due to overlap with more dominant features from H_{II} and H_{III}. The weakest feature is just above the noise level and belongs to the same ridge H_{IV}. Although the feature is too weak to be observed in the presence of much more intense and closely located ridges from the H_I protons in protonated buffer, it is visible upon subtraction of the two 2D ^1H HYSCORE spectra. Figure 5S shows the difference spectrum in Figure 4S plotted in frequency-squared coordinates. As expected, all three spectral features lie in a single straight line confirming the conclusion that these features belong to the same proton ridge.

To obtain additional information on the binding of acetate ions to **1**, we perform 2D ^{13}C HYSCORE spectroscopy in buffer containing sodium acetate enriched with ^{13}C at the carbonyl carbon atom. Figure 4 shows the 2D difference HYSCORE spectrum between ^{13}C-labeled and natural abundance ^{13}C acetate buffer. There are two partially overlapped ridges, $^{13}C_I$ and $^{13}C_{II}$, that are observed in the spectrum. In frequency-squared coordinates, the ridge $^{13}C_I$ represents a segment of a straight line as expected from a nucleus with a well-defined hyperfine interaction. From the slope and the intercept of the ridge $^{13}C_I$ in frequency-squared coordinates, we obtain isotropic

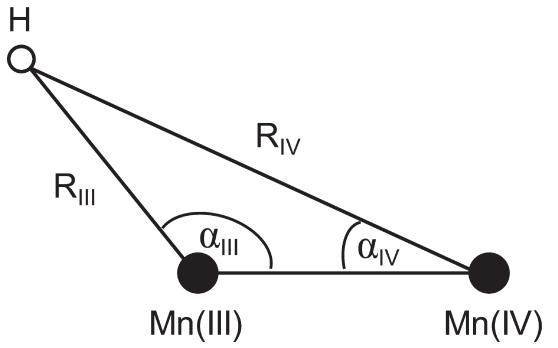

Figure 5. Diagram depicting the distances, R_{III}, R_{IV}, and the angles, α_{III} and α_{IV}, that are used in the eqs 2−7.

and anisotropic hyperfine parameters, a_{iso} and T, of ±1.4 and ±3.5 MHz or ∓4.9, respectively. The second ridge, $^{13}C_{II}$, is curved along the antidiagonal, and it is not a straight line in frequency-squared coordinates. This ridge originates from non-specific matrix hyperfine interactions.

DISCUSSION

Theory. Previous ENDOR spectroscopy studies of mixed-valence Mn(III)Mn(IV) complexes[28,31] have shown that the anisotropic dipolar component of the hyperfine interaction between the unpaired electrons of the paramagnetic dimanganese di-μ-oxo core and the surrounding proton nuclei can be estimated by a simple point-dipole approximation. In these studies, it was assumed that the electron spin density is localized entirely on manganese ions and the electron spin state of the Mn(III) and Mn(IV) ion are pure $S = 2$ and $S = 3/2$, respectively. In this case, the three dipolar components of the proton hyperfine tensor $[A_x, A_y, A_z]$ can be calculated using the equations:[29,31]

$$A_x = (1/2)(p_{III}T_{III} + p_{IV}T_{IV} - 3\Gamma) \quad (2)$$

$$A_y = -(p_{III}T_{III} + p_{IV}T_{IV}) \quad (3)$$

$$A_z = (1/2)(p_{III}T_{III} + p_{IV}T_{IV} + 3\Gamma) \quad (4)$$

where

$$\Gamma = [(p_{III}T_{III})^2 + (p_{IV}T_{IV})^2 + 2p_{III}p_{IV}T_{III}T_{IV}\cos(2\alpha_{III} + 2\alpha_{IV})]^{1/2}$$

and

$$T_{III} = \frac{g_e\beta_e g_N\beta_N}{hR_{III}^2} \quad \text{and} \quad T_{IV} = \frac{g_e\beta_e g_N\beta_N}{hR_{IV}^2}$$

Here, β_e, β_N, g_e, and g_N are the Bohr magneton, nuclear magneton, electron, and nuclear g-factors, respectively. As shown in Figure 5, R_{III} and R_{IV} are the distances from proton to the Mn(III) and Mn(IV) ion, respectively, and α_{III} and α_{IV} are the angles between the vectors connecting the proton with the corresponding manganese ion and the vector connecting two manganese ions, respectively. p_{III} and p_{IV} are the spin projection factors for the Mn(III) and Mn(IV) ion, respectively. In general, the projection factors depend on the strength of the exchange coupling between the ions as well as the zero-field splitting

Table 1. Metric Parameters and Corresponding Calculated Hyperfine Components of the Four Protons That Are Closest to the Dimanganese "Di-μ-oxo" Core of 1

	(R_{III}, R_{IV}), Á	(α_{III},α_{IV}), deg	(A_x, A_y, A_z), MHz	T, MHz
1	(3.14, 3.91)	(83, 53)	(−6.0, −3.8, 9.7)	4.9
2	(3.16, 3.89)	(82, 54)	(−5.9, −3.7, 9.6)	4.8
3	(3.89, 3.16)	(54, 82)	(−5.3, −0.2, 5.5)	2.8
4	(3.91, 3.14)	(83, 53)	(−5.4, −0.1, 5.5)	2.7

(ZFS) interaction of each manganese ion. However, using the approximation that in μ-oxo-bridged systems the exchange coupling constant is much larger than any of the ZFS parameters,[43] $p_{III} \approx 2$ and $p_{IV} \approx -1$ and the eqs 2−4 can be simplified to[28]

$$A_x = (1/2)(2T_{III} - T_{IV} - 3\Gamma) \quad (5)$$

$$A_y = -(2T_{III} - T_{IV}) \quad (6)$$

$$A_z = (1/2)(2T_{III} - T_{IV} + 3\Gamma) \quad (7)$$

where

$$\Gamma = [4T_{III}^2 + T_{IV}^2 - 4T_{III}T_{IV}\cos(2\alpha_{III} + 2\alpha_{IV})]^{1/2}$$

In the 2D ^{1}H HYSCORE spectrum of **1** in aqueous protonated buffer, we observe hyperfine interactions with four types of protons, namely, H_I−H_{IV}, that are magnetically interacting with the unpaired electrons of the paramagnetic dimanganese di-μ-oxo core. For each group of protons, we obtain four sets of possible hyperfine parameters. To assign the groups of observed protons and discriminate among the four sets of hyperfine components, we consider the relation between the geometric structure that is known from X-ray crystallography and the hyperfine parameters obtained in this study.

Table 1 lists the distances R_{III}, R_{IV} and angles α_{III}, α_{IV} of the four nearest protons of the terpyridine ligands taken from the crystal structure of **1**[26] and the three hyperfine components of the corresponding hyperfine tensors that were calculated using the expressions 5−7. Two of the four protons are located proximal to the Mn(III) ion and display nearly axial and almost identical hyperfine tensors. The other two protons that are located proximal to the Mn(IV) ion are almost identical as well, but their interaction is highly rhombic. To compare the calculated and experimental data, we estimate the anisotropic hyperfine parameter, T, for the rhombic tensors listed in the Table 1 using the following representation of the hyperfine tensor

$$(A_x, A_y, A_z) = (a_{iso} - T(1-\delta), a_{iso} - T(1+\delta), a_{iso} + 2T) \quad (8)$$

where the rhombicity parameter must satisfy the condition $-1 \leq \delta \leq 1$. For the pair of protons that are proximal to the Mn(III) ion, we obtain T values of 4.9 and 4.8 MHz. For the pair of protons that are proximal to the Mn(IV) ion, we obtain T values of 2.8 and 2.7 MHz. From the spectral resolution of the 2D ^{1}H HYSCORE measurements in this study, we are unable to distinguish between the protons within each pair, and, thus, we compare the average T of each pair with the experimental values.

Assignment of H_I Protons. H_I is the only nonexchangeable group of protons that are observed in the experimental spectrum of **1**. The absolute value of T that is obtained for the hyperfine interaction with the H_I group of protons is in agreement with the absolute value for the average T that is calculated for the protons that are proximal to the Mn(III) ion of **1**. In comparison, the absolute value of T that is calculated for the protons that are proximal to the Mn(IV) ion of **1** is significantly smaller than the hyperfine interaction that is measured for the H_I group of protons. Thus, we conclude that H_I is the proximal pair of protons of the terpyridine ligand that is coordinated to the Mn(III) ion.

This assignment allows us to discriminate between the two possible signs of T that are obtained from the experimental spectrum. The sign of T must be positive to agree with the calculated value. The positive sign is due to a dominant contribution from the Mn(III) ion with a positive spin projection factor, p_{III}, of 2. The other pair belonging to the terpyridine ligand that is coordinated to the Mn(IV) ion is not observed in the experimental 2D ^{1}H HYSCORE spectra in this study. The hyperfine interaction of these protons is highly rhombic in nature, distributing the ^{1}H HYSCORE cross-peaks over a much larger area in 2D frequency space. This significantly reduces the intensity of the peaks and precludes experimental detection.

To verify the assignment of the H_I protons, we perform 2D ^{1}H HYSCORE measurements of **2**. In **2**, there are no terminal water molecules that are directly coordinated to the manganese ions. Previous ENDOR spectroscopy studies have demonstrated that only the nearest eight protons of the bipyridine ligands contribute to the experimentally observed proton hyperfine interactions.[28] The eight protons are divided into two groups of four protons. The first group of protons is much closer to the Mn(III) ion, and the second group of protons is closer to the Mn(IV) ion. The group of protons that is proximal to the Mn(III) ion has a nearly axial hyperfine tensor, and the group of protons that is proximal to the Mn(IV) ion has one pair of protons with a highly rhombic tensor and another pair with a hyperfine interaction that is too small to be detected by 2D ^{1}H HYSCORE spectroscopy.[44] Similar to what is observed with **1**, we observe a single ridge with the anisotropic hyperfine parameter, T, corresponding to the average value of the four protons that are proximal to the Mn(III) ion of **2**. We do not detect ridges arising from hyperfine interaction(s) with the protons that are proximal to the Mn(IV) ion of **2**. This confirms our previous assignment of H_I as arising from hyperfine interactions with the two protons from the terpyridine ligand that is coordinated to the Mn(III) ion of **1**.

It is important to mention that in both **1** and **2** there are multiple intrinsic protons on the ligand that are located farther from the manganese ions. We performed calculations using the eqs 5−7 that yield values of T that are less than 1.1 MHz. Hence, it is not possible to distinguish the remote protons on the ligand from the nonspecific matrix protons. The remote protons on the ligand likely contribute to the diagonal feature located at the Zeeman frequency.

In the case of **1**, for a given positive value of T of 4.1 MHz, there are still two possible values of a_{iso}, namely, 1.1 and −5.2 MHz. The second value is too large and would require a strong delocalization of electron spin density toward the terpyridine ligand in **1**. Such delocalization would contradict quantum chemical calculations performed on similar systems.[45,46] The hyperfine parameters that are obtained for the H_I protons in this study are in agreement with previous studies.[28,31]

Assignment of H_{II-IV} Protons. In addition to H_I, we observe three types of exchangeable protons, H_{II}−H_{IV}, in the 2D ^{1}H

Table 2. Experimentally Determined Anisotropic and Isotropic Components of the Proton Hyperfine Interactions of 1 in Aqueous Buffer

	H_I	H_{II}	H_{III}	H_{IV}
a_{iso}, MHz	1.1 ± 0.3	−2.1 ± 0.2, 4.5 ± 0.2	−1.9 ± 0.2, 3.5 ± 0.2	2.5 ± 0.4
T, MHz	4.1 ± 0.3	−2.4 ± 0.2	−1.7 ± 0.2	7.3 ± 0.4

HYSCORE spectrum of **1**. These protons are assigned to water molecules that are present in the vicinity of the two manganese ions. The nonzero isotropic hyperfine component of these protons (Table 2) requires the presence of substantial electron spin density on the corresponding oxygen atom. Thus, $H_{II}-H_{IV}$ must arise from a water molecule that is directly interacting with the dimanganese di-μ-oxo core of **1**.

Careful assessment of the X-ray crystal structure of **1** indicates that there are three such water molecules (Figure 1A).[26] There are two terminal water molecules that are directly coordinated to the Mn(III) and Mn(IV) ion, and there is one water molecule that is H-bonded to the oxygen atom of a μ-oxo bridge of **1**. We can confidently exclude the assignment of $H_{II}-H_{IV}$ to the H-bonded water molecule as the numerically estimated value of T disagrees with the experimentally measured value of T. Also, calculations indicate that the hyperfine tensor of the proton H-bonded to the μ-oxo bridge is highly rhombic, and, thus, these hyperfine interactions are strongly suppressed in the 2D ^{1}H HYSCORE spectrum.

The protons $H_{II}-H_{IV}$ belong to the two terminal water molecules that are directly coordinated to the Mn(III) and Mn(IV) ion of **1**. The two water molecules can be easily differentiated as the location of the oxygen atom of these water molecules is known from the X-ray crystal structure (Figure 1A) and the estimates of the anisotropic components differ significantly. Using known positions of the oxygen atoms in the X-ray crystal structure of **1** and a O−H bond length of 1 Å, we find that the dominant contribution to the proton hyperfine tensor is from the proximal manganese atom. The substantial difference between the Mn(III) and Mn(IV) ions originates from the difference in the magnitude of the respective spin projection factors. First, at equal distances the magnetic interaction with the Mn(III) ion results in a hyperfine interaction that is twice as large in comparison with the Mn(IV) ion. Second, the sign of the projection factors is opposite. The reduction of the hyperfine interaction at the Mn(IV) ion due to the presence of the neighboring Mn(III) ion must be twice the reduction at the Mn(III) site due to the presence of the Mn(IV) ion. Thus, taking these factors into account, the absolute magnitude of the dipolar interaction is expected to be much smaller at the Mn(IV) ion. Therefore, H_{IV} is assigned to a terminal water molecule that is coordinated at the Mn(III) ion, while the protons H_{II} and H_{III} are assigned to the terminal water molecule that is coordinated at the Mn(IV) ion.

In this study, we successfully resolve hyperfine interactions with the two water protons at the Mn(IV) ion. However, the spectral resolution is not sufficient to resolve the hyperfine interactions with the two water protons at the Mn(III) ion of **1**. This is because a much smaller contribution from the Mn(IV) ion results in a weaker dependence of the hyperfine interaction on the orientation of the water molecule bound to the Mn(III) ion with respect to Mn−Mn axis. The two protons are expected to be at approximately equal distances from the coordinating ion, and therefore only the second ion could contribute to the difference in the size of their anisotropic hyperfine interaction (see the Supporting Information).

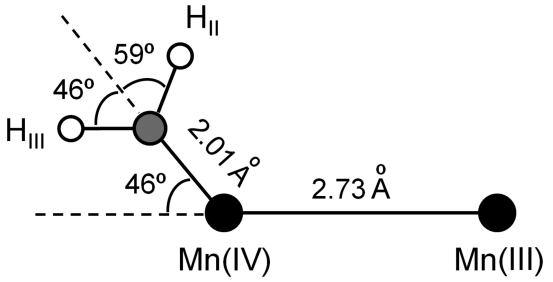

Figure 6. Proposed orientation of the water molecule of **1** in acetate buffer with respect to the dimanganese di-μ-oxo core.

In addition, the size of the anisotropic hyperfine interaction depends on the inverse cube of the distance $(1/r^3)$ between the proton nuclear spin and the unpaired electron spin. From the X-ray crystal structure, the average distance between the oxygen atom on a water molecule and the corresponding manganese ion is 2.01 Å. Even a small deviation from this value would result in a significant change in the hyperfine interaction. Using corrected values of $p_{III} = 1.915$ and $p_{IV} = 0.86$ in the eqs 2−4 and assuming that the angle between two O−H bonds is equal to 105°, we compare the calculated values of the anisotropic hyperfine components with the measured values for all of the possible orientations of the water molecule with respect to the Mn(III)−Mn(IV) axis. The best agreement is achieved when the two water protons lie in the plane defined by the oxygen atom on the water and the two manganese ions and the angle between the O−H bonds and O−Mn(IV) bond is 46° and 59° for H_{III} and H_{II} protons, respectively (Figure 6). The corresponding absolute values of T in this geometry are calculated to be 2.2 MHz for H_{III} and 2.9 MHz for H_{II}.

Taking into account the assignment of the $H_{II}-H_{IV}$ group of protons, we can easily discriminate between the possible signs of the T value for all three protons. The sign must be positive for H_{IV} and negative for H_{II} and H_{III}. We can also exclude the parameter set of H_{IV} corresponding to an a_{iso} value of −9.8 MHz, since a large isotropic hyperfine component contradicts the data in previous literature. Previous ENDOR spectroscopy studies demonstrated that the protons of the water molecule that is coordinated at a Mn(III) ion have isotropic hyperfine components of ∼1−3 MHz.[29] While the parameter set with an a_{iso} value of 2.5 MHz in the present study agrees well with the results of the ENDOR study, an a_{iso} value of −9.8 MHz is unreasonable. Given the negative sign of T for the H_{II} and H_{III} protons, there are still two possible sets of a_{iso} values for each proton. The a_{iso} values have opposite signs but are comparable in their absolute values. At this stage we cannot discriminate between the parameter sets, and we consider both as possible options. Table 2 summarizes the final sets of hyperfine parameters for the H_I-H_{IV} group of protons.

Replacement of the Water Ligand of 1 With Acetate. Upon comparison of the 2D ^{1}H HYSCORE spectra measured in aqueous (Figure 3A) and acetate buffer (Figure 3D), we observe that the ridges corresponding to the H_{IV} protons disappear when acetate binds to **1**. Since we unambiguously assigned H_{IV} to the water molecule that is coordinated at the Mn(III) ion, we

conclude that the acetate ion replaces this water molecule while the second water molecule remains coordinated to the Mn(IV) ion of **1** in the presence of acetate ions. While the absolute values of a_{iso} that are measured for H_{IV} in this study are similar to those for H_{II} and H_{III}, the "true" isotropic couplings that are divided by the corresponding projection factor are smaller for H_{IV} in comparison with H_{II} and H_{III}. The smaller values might reflect a weaker metal−ligand interaction and, thus, a lower binding energy for the terminal water molecule that is coordinated at the Mn(III) ion.

Additional support of acetate binding to the Mn(III) ion is based on the hyperfine parameters obtained for the hyperfine coupling, $^{13}C_I$, that is observed in the 2D ^{13}C HYSCORE spectrum. The value of the anisotropic hyperfine component, T, of 1.4 MHz is too large to be attributed to an acetate ion coordinated at the Mn(IV) ion. In contrast, this value agrees very well with the corresponding value of T = 7.3 MHz for the H_{IV} protons taking into account the ratio of nuclear g-factors as well as the slightly longer length of the C−O bond in acetate in comparison with the O−H bond length of water. This provides additional support that an acetate ion binds at the Mn(III) ion.

From the 2D ^{13}C HYSCORE spectrum, we observe that some of the manganese dimers magnetically interact with at least one ^{13}C nucleus that has a much smaller anisotropic hyperfine component. It is possible that the ^{13}C-labeled carbonyl carbon atom of the acetate ion that is bound to the Mn(IV) ion partially contributes to the second experimental ridge, $^{13}C_{II}$. Taking into account the much larger relative intensity of the $^{13}C_I$ with respect to $^{13}C_{II}$ and the fact that only the ridge H_{IV} disappears in the presence of acetate ions, we conclude that the fraction of acetate ions that are coordinated at the Mn(IV) ion is either very small or completely absent in the solution.

We observe that the isotropic hyperfine interaction, a_{iso}, that is measured for carbonyl ^{13}C-labeled acetate has values of 3.5 and −4.9 MHz (set of parameters corresponding to positive value of T is chosen). This corresponds to a much larger electron spin density at the carbon atom in comparison with the hydrogen atoms of the water ligands. The higher electron spin density might be due to partial C−O bond conjugation of the carbonyl group, but it could also reflect partial covalent character of the bond between acetate and the Mn(III) ion.

This study provides direct evidence that only one acetate ion is bound to **1** in solution. This is in agreement with the study conducted by Brudvig and co-workers that examines the effect of acetate titration on oxidation potential of **1** using cyclic voltammetry[34] where the authors demonstrate that the oxidation potential was reduced from 1.3 to 1.1 V NHE upon the formation of a 1:1 complex of acetate and the Mn(III)Mn(IV) complex and that this does not change upon further increase of acetate concentration.[34]

In addition, as can be seen from a comparison of parameters listed in Tables 1S and 2S, the hyperfine components remain virtually unchanged upon acetate binding to **1**. Since the anisotropic hyperfine components are sensitive to the geometry and the isotropic hyperfine components are sensitive to the electronic structure of the dimanganese di-μ-oxo complex, we conclude that a significant structural change is not induced upon replacement of the water ligand of **1** with an acetate ion.

Relevance to the Structure of PSII. The proton environment of the OEC of PSII has been previously studied by ENDOR and ESEEM spectroscopy.[19,21] Although these studies have yielded important structural information, the precise nature of the substrate water molecules bound to the manganese ions in the OEC could not be inferred by ENDOR and ESEEM spectroscopy. Scarce spectroscopic data on the protons of water molecules and hydroxy groups that are coordinated at Mn(III) and Mn(IV) ions are among the major factors that limit a better understanding of the environment of the bound substrate water molecules in the OEC of PSII.

Previous ENDOR and ESEEM spectroscopy studies have obtained proton hyperfine parameters of a water molecule that is coordinated at a Mn(III) ion.[29] The values of the hyperfine parameters that were obtained are similar to the values obtained in our study. However, there is a lack of experimental data on hyperfine interactions with the protons of a water or hydroxyl group that is coordinated at a Mn(IV) ion. Hence, the results obtained in the present study are aimed at creating an experimental database of hyperfine parameters.

Due to its ability to act as a functional water oxidation catalyst, the dimaganese di-μ-oxo complex, **1**, is an excellent biomimetic model for the OEC of PSII.[26,27] In **1**, the terminal water molecules are coordinated in equatorial positions on the dimanganese di-μ-oxo core. Since spectroscopic hyperfine parameters might depend on the coordination geometry, we are pursuing experimental studies to differentiate axial and equatorial ligation to obtain a better understanding of the available data on the OEC of PSII. The results obtained in this work as well as in the earlier studies[29] show that for equatorially coordinated water ligands, the isotropic hyperfine constants, a_{iso}, for protons are on the order of 1−5 MHz and these are comparable for both the Mn(III) and Mn(IV) ions. While the value of a_{iso} is unlikely to change significantly for axially coordinated water molecules in the case of the Mn(IV) ion due to its higher symmetry, it might increase in the case of the Mn(III) oxidation state.[24] The presence of a nonzero isotropic hyperfine interaction could be used to discriminate between the water molecules directly coordinated to manganese ions and those that are in the vicinity but not coordinated to either the Mn(III) or Mn(IV) ion. In contrast, the value of the anisotropic component, T, differs significantly. This reflects a pronounced difference in the spin projection factors of the Mn(III) ion versus the Mn(IV) ion. Since similar spin projection factors are expected for the manganese ions in the OEC,[47] the differentiation between these two coordination possibilities can be performed based on a comparison of the anisotropic component of the corresponding hyperfine interaction.

SUMMARY

In this study, we quantitatively characterize the magnetic interactions between the unpaired electrons and protons of terminal water ligands in the mixed-valence dimanganese di-μ-oxo complex **1**. There are two protons of the water molecule coordinated at the Mn(III) ion that are magnetically equivalent within our experimental resolution, and these protons have anisotropic and isotropic hyperfine components, T and a_{iso}, of 7.3 and 2.5 MHz, respectively. The anisotropic hyperfine components for magnetically distinct protons belonging to the water molecule that is coordinated at the Mn(IV) ion are −1.7 and −2.4 MHz. These values correspond to two sets of possible isotropic components, a_{iso}, with values of −2.1, 4.5 MHz or −1.9, 3.5 MHz, respectively. The large difference in the measured values of T for two oxidation states of the manganese ion could be explained in terms of spin projection factors of

approximately 2 and −1 for the Mn(III) and Mn(IV) ion, respectively. While calculations using a point-dipole approximation yield satisfactory agreement for a water molecule coordinated at the Mn(III) ion, spin delocalization is found to be an important factor in interpreting the dipolar coupling in the case of the water molecule coordinated at the Mn(IV) ion. The measured hyperfine values provide an important frame of reference for understanding similar spectroscopic data of the OEC of PSII. Further, the 2D ^{1}H and ^{13}C HYSCORE spectroscopy measurements in the presence of acetate buffer provide direct experimental evidence that an acetate ion binds at the Mn(III) ion and replaces the corresponding water ligand of **1**.

■ ASSOCIATED CONTENT

Supporting Information. Description of the linear analysis of proton hyperfine interactions of dimanganese di-μ-oxo mimics of the oxygen-evolving complex of photosystem II and electron-spin−echo detected field sweep EPR and 2D HYSCORE spectra of **1**. This material is available free of charge via the Internet at http://pubs.acs.org.

■ AUTHOR INFORMATION

Corresponding Author

*Phone (518) 276 3271; fax (518) 276 4887; e-mail lakshk@rpi.edu.

■ ACKNOWLEDGMENT

This study is supported by the Solar Energy Utilization Program, Office of Basic Energy Sciences, U.S. Department of Energy under the contract DE-FG02-10ER15903.

■ REFERENCES

(1) Zouni, A.; Witt, H. T.; Kern, J.; Fromme, P.; Krauss, N.; Saenger, W.; Orth, P. *Nature* **2001**, *409*, 739–743.
(2) Guskov, A.; Kern, J.; Gabdulkhakov, A.; Broser, M.; Zouni, A.; Saenger, W. *Nat. Struct. Mol. Biol.* **2009**, *16*, 334–342.
(3) Kamiya, N.; Shen, J. R. *Proc. Natl. Acad. Sci. U.S.A.* **2003**, *100*, 98–103.
(4) Ferreira, K. N.; Iverson, T. M.; Maghlaoui, K.; Barber, J.; Iwata, S. *Science* **2004**, *303*, 1831–1838.
(5) Löll, B.; Kern, J.; Saenger, W.; Zouni, A.; Biesiadka, J. *Nature* **2005**, *438*, 1040–1044.
(6) Yano, J.; Kern, J.; Sauer, K.; Latimer, M. J.; Pushkar, Y.; Biesiadka, J.; Loll, B.; Saenger, W.; Messinger, J.; Zouni, A.; Yachandra, V. K. *Science* **2006**, *314*, 821–825.
(7) Kern, J.; Biesiadka, J.; Löll, B.; Saenger, W.; Zouni, A. *Photosynth. Res.* **2007**, *92*, 389–405.
(8) Kok, B.; Forbush, B.; McGloin, M. *Photochem. Photobiol.* **1970**, *11*, 457–475.
(9) Brudvig, G. W. In *Mechanistic Bioinorganic Chemistry*; Thorp, H. H., Pecoraro, V. L., Eds. Advances in Chenistry Series No. 246; Oxford University Press: New York, 1995; pp 249−263.
(10) Lakshmi, K. V.; Eaton, S. S.; Eaton, G. R.; Frank, H. A.; Brudvig, G. W. *J. Phys. Chem. B* **1998**, *102*, 8327–8335.
(11) Lakshmi, K. V.; Eaton, S. S.; Eaton, G. R.; Brudvig, G. W. *Biochemistry* **1999**, *38*, 12758–12767.
(12) Peloquin, J. M.; Britt, R. D. *Biochim. Biophys. Acta Bioenerg.* **2001**, *1503*, 96–111.
(13) Messinger, J.; Nugent, J. H. A.; Evans, M. C. W. *Biochemistry* **1997**, *36*, 11055–11060.
(14) Ahrling, K. A.; Peterson, S.; Styring, S. *Biochemistry* **1998**, *37*, 8115–8120.
(15) Kulik, L. V.; Epel, B.; Lubitz, W.; Messinger, J. *J. Am. Chem. Soc.* **2005**, *127*, 2392–2393.
(16) Yachandra, V. K.; Sauer, K.; Klein, M. P. *Chem. Rev.* **1996**, *96*, 2927–2950.
(17) Yano, J.; Pushkar, Y.; Glatzel, P.; Lewis, A.; Sauer, K.; Messinger, J.; Bergmann, U.; Yachandra, V. *J. Am. Chem. Soc.* **2005**, *127*, 14974–14975.
(18) Haddy, A.; Lakshmi, K. V.; Brudvig, G. W.; Frank, H. A. *Biophys. J.* **2004**, *87*, 2885–2896.
(19) Su, J. H.; Messinger, J. *Appl. Magn. Reson.* **2010**, *37*, 123–136.
(20) Kawamori, A.; Inui, T.; Ono, T.; Inoue, Y. *FEBS Lett.* **1989**, *254*, 219–224.
(21) Yamada, H.; Mino, H.; Itoh, S. *Biochim. Biophys. Acta Bioenerg.* **2007**, *1767*, 197–203.
(22) Aznar, C. P.; Britt, R. D. *Philos. Trans. R. Soc. London, Ser. B.* **2002**, *357*, 1359–1365.
(23) Britt, R. D.; Campbell, K. A.; Peloquin, J. M.; Gilchrist, M. L.; Aznar, C. P.; Dicus, M. M.; Robblee, J.; Messinger, J. *Biochim. Biophys. Acta Bioenerg.* **2004**, *1655*, 158–171.
(24) Tang, X. S.; Sivaraja, M.; Dismukes, G. C. *J. Am. Chem. Soc.* **1993**, *115*, 2382–2389.
(25) Fiege, R.; Zweygart, W.; Bittl, R.; Adir, N.; Renger, G.; Lubitz, W. *Photosyn. Res.* **1996**, *48*, 227–237.
(26) Limburg, J.; Vrettos, J. S.; Liable-Sands, L. M.; Rheingold, A. L.; Crabtree, R. H.; Brudvig, G. W. *Science* **1999**, *283*, 1524–1527.
(27) Chen, H. Y.; Tagore, R.; Das, S.; Incarvito, C.; Faller, J. W.; Crabtree, R. H.; Brudvig, G. W. *Inorg. Chem.* **2005**, *44*, 7661–7670.
(28) Randall, D. W.; Chan, M. K.; Armstrong, W. H.; Britt, R. D. *Mol. Phys.* **1998**, *95*, 1283–1294.
(29) Randall, D. W.; Gelasco, A.; Caudle, M. T.; Pecoraro, V. L.; Britt, R. D. *J. Am. Chem. Soc.* **1997**, *119*, 4481–4491.
(30) Tan, X. L.; Gultneh, Y.; Sarneski, J. E.; Scholes, C. P. *J. Am. Chem. Soc.* **1991**, *113*, 7853–7858.
(31) Schafer, K. O.; Bittl, R.; Zweygart, W.; Lendzian, F.; Haselhorst, G.; Weyhermuller, T.; Wieghardt, K.; Lubitz, W. *J. Am. Chem. Soc.* **1998**, *120*, 13104–13120.
(32) Cooper, S. R.; Calvin, M. *J. Am. Chem. Soc.* **1977**, *99*, 6623–6630.
(33) Tagore, R.; Chen, H. Y.; Crabtree, R. H.; Brudvig, G. W. *J. Am. Chem. Soc.* **2006**, *128*, 9457–9465.
(34) Cady, C. W.; Shinopoulos, K. E.; Crabtree, R. H.; Brudvig, G. W. *Dalton Trans.* **2010**, *39*, 3985–3989.
(35) Kasumaj, B.; Stoll, S. *J. Magn. Reson.* **2008**, *190*, 233–247.
(36) Song, R.; Zhong, Y. C.; Noble, C. J.; Pilbrow, J. R.; Hutton, D. R. *Chem. Phys. Lett.* **1995**, *237*, 86–90.
(37) Dikanov, S. A.; Bowman, M. K. *J. Magn. Reson., Ser. A* **1995**, *116*, 125–128.
(38) Stoll, S.; Calle, C.; Mitrikas, G.; Schweiger, A. *J. Magn. Reson.* **2005**, *177*, 93–101.
(39) Weyers, A. M.; Chatterjee, R.; Milikisiyants, S.; Lakshmi, K. V. *J. Phys. Chem. B* **2009**, *113*, 15409–15418.
(40) Cooper, S. R.; Dismukes, G. C.; Klein, M. P.; Calvin, M. *J. Am. Chem. Soc.* **1978**, *100*, 7248–7252.
(41) Brewer, K. J.; Calvin, M.; Lumpkin, R. S.; Otvos, J. W.; Spreer, L. O. *Inorg. Chem.* **1989**, *28*, 4446–4451.
(42) Wang, T.; Brudvig, G.; Batista, V. S. *J. Chem. Theory Comput.* **2010**, *6*, 755–760.
(43) Zheng, M.; Khangulov, S. V.; Dismukes, G. C.; Barynin, V. V. *Inorg. Chem.* **1994**, *33*, 382–387.
(44) Peloquin, J. M.; Campbell, K. A.; Britt, R. D. *J. Am. Chem. Soc.* **1998**, *120*, 6840–6841.
(45) Schinzel, S.; Kaupp, M. *Can. J. Chem.* **2009**, *87*, 1521–1539.
(46) Sproviero, E. M.; Gascon, J. A.; McEvoy, J. P.; Brudvig, G. W.; Batista, V. S. *J. Inorg. Biochem.* **2006**, *100*, 786–800.
(47) Peloquin, J. M.; Campbell, K. A.; Randall, D. W.; Evanchik, M. A.; Pecoraro, V. L.; Armstrong, W. H.; Britt, R. D. *J. Am. Chem. Soc.* **2000**, *122*, 10926–10942.